nature genetics

A mouse model of ATR-Seckel shows embryonic replicative stress and accelerated aging

Matilde Murga[1], Samuel Bunting[2], Maria F Montaña[1], Rebeca Soria[1], Francisca Mulero[3], Marta Cañamero[4], Youngsoo Lee[5], Peter J McKinnon[5], Andre Nussenzweig[2] & Oscar Fernandez-Capetillo[1]

Although DNA damage is considered a driving force for aging, the nature of the damage that arises endogenously remains unclear. Replicative stress, a source of endogenous DNA damage, is prevented primarily by the ATR kinase. We have developed a mouse model of Seckel syndrome characterized by a severe deficiency in ATR. Seckel mice show high levels of replicative stress during embryogenesis, when proliferation is widespread, but this is reduced to marginal amounts in postnatal life. In spite of this decrease, adult Seckel mice show accelerated aging, which is further aggravated in the absence of p53. Together, these results support a model whereby replicative stress, particularly *in utero*, contributes to the onset of aging in postnatal life, and this is balanced by the replicative stress–limiting role of the checkpoint proteins ATR and p53.

The accumulation of DNA damage can have important consequences that limit the lifespan of mammalian organisms, such as aging or cancer. Concerning aging, one current theory is based on the accumulation of DNA damage[1]. In accordance with this theory, signals indicating activation of the so-called DNA damage response (DDR) have been shown to increase in aged tissues and stem cells[2,3], and several mouse models with impaired DNA repair show features of premature aging[4]. Concerning cancer, DNA damage is the source of mutations that drive malignant transformation. Therefore, it is not surprising that organisms have evolved complex signaling pathways to protect their DNA. In particular, the DDR starts with the activation of either one of two members of the PIKK family of protein kinases: Ataxia Telangiectasia Mutated (ATM) and Ataxia Telangiectasia and Rad3-related (ATR)[5]. Whereas ATM is activated by DNA double-strand breaks (DSBs), ATR responds to single-stranded DNA (ssDNA) both at resected DSBs and at aberrant replicative structures that compromise genome integrity during the S phase of the cell cycle. Regardless of the kinase that initiates the signaling, the final outcome of the DDR is to promote DNA repair while delaying cell cycle progression until chromosomes are repaired.

Whereas ATM-deficient mice were generated more than a decade ago[6–8], efforts to decipher the physiological roles of ATR have been hampered by the essential nature of this kinase[9,10]. However, although complete knockout of *Atr* is lethal, a seminal study found a hypomorphic mutation in humans with a rare disease known as Seckel syndrome (MIM210600)[11]. This disease was first described by Helmut Seckel in 1960 as "bird-headed dwarfism" because of the severe dwarfism and craniofacial features of those affected[12]. In homozygosity, the mutation introduces a splicing defect that reduces the abundance of ATR to almost undetectable, yet the remaining protein is sufficient for viability. We have here exploited the human *ATR*-Seckel mutation to generate a viable model for the study of ATR function in mammals.

RESULTS

Strategy to develop a mouse model of Seckel

One of the mutations that has been linked to Seckel syndrome is a synonymous A>G transition in exon 9 of the *ATR* gene[11]. The mutation promotes the skipping of this exon during the splicing reaction, which results in a severe ATR hypomorphism. We decided to use this information to generate a mouse model of the human disease. We reasoned that because the Seckel mutation affects splicing, the introns and splicing donor/acceptor sequences encompassing *ATR* exon 9 were likely to be necessary to recapitulate the molecular defect. Thus, our strategy was to swap the entire mouse genomic fragment encompassing exons 8, 9 and 10 with the human counterpart and then introduce the Seckel mutation to the humanized mouse allele (ATR^{S}; **Fig. 1a,b**). $ATR^{S/S}$ mouse embryonic fibroblasts (MEFs) showed a severe splicing deficiency of the humanized transcript at the exon 8–10 region that led to a deficit of ATR protein comparable to that observed in human ATR-Seckel cells (**Fig. 1c–f**). Sequencing of the main splicing product of $ATR^{S/S}$ MEFs revealed that it corresponded to an aberrant transcript that had skipped exon 9. Thus, the molecular behavior of the humanized mouse allele faithfully recapitulated that of the mutant *ATR* gene previously linked to Seckel syndrome.

[1]Genomic Instability Group, Spanish National Cancer Research Centre (CNIO), Madrid, Spain. [2]Experimental Immunology Branch, National Cancer Institute, National Institutes of Health, Bethesda, Maryland, USA. [3]Molecular Imaging Unit, CNIO, Madrid, Spain. [4]Comparative Pathology Unit, CNIO, Madrid, Spain. [5]Department of Genetics and Tumor Cell Biology, St. Jude Children's Research Hospital, Memphis, Tennessee, USA. Correspondence should be addressed to M.M. (mmurga@cnio.es) or O.F.-C. (ofernandez@cnio.es).

Received 21 January; accepted 23 June; published online 20 July 2009; doi:10.1038/ng.420

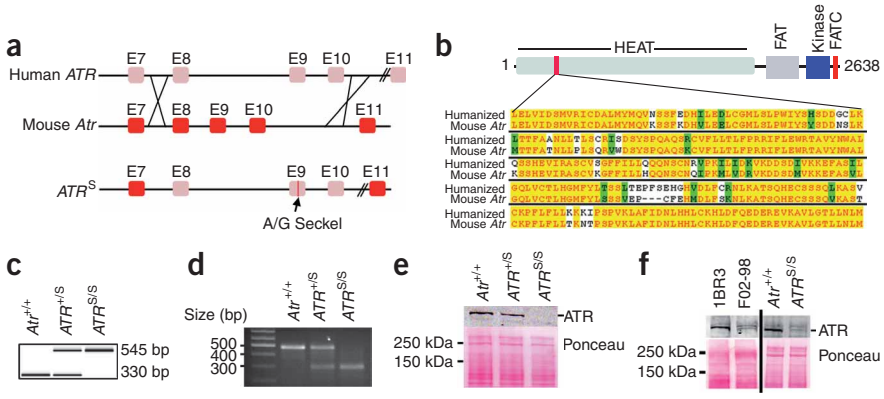

Figure 1 Generation of a humanized allele of Seckel syndrome. (**a**) Strategy for generating the mutant allele. The rearranged allele contains the genomic region encompassing human exons (E) 8–10 (pink) inserted into the equivalent region of the mouse *Atr* gene (red exons). The Seckel syndrome mutation is indicated in E9. (**b**) The location and sequence homology of the humanized ATR protein in the region encoded in E8–E10. The full-length chimeric protein, domain structure shown above, has 99.1% homology with mouse ATR. (**c**–**e**) Analysis of littermate MEF lines by PCR genotyping (**c**), RT-PCR of ATR with primers at E8 and E10 (**d**) and ATR protein blotting (**e**). (**f**) ATR protein blot in human fibroblast lines 1BR3 (control) and F02-98 (Seckel), together with $Atr^{+/+}$ and $ATR^{S/S}$ MEFs.

Recapitulation of Seckel syndrome in $ATR^{S/S}$ mice

$ATR^{S/S}$ mice were born at submendelian ratios (χ^2, $P < 0.0001$; 31.8% $Atr^{+/+}$, 57.8% $ATR^{S/+}$, 10.4% $ATR^{S/S}$) and showed severe dwarfism that was already noticeable at birth (**Fig. 2a–d**). Of note, mutant placentas showed an accumulation of necrotic areas and overall loss of cellularity, which could also contribute to the dwarf phenotype regardless of intrinsic developmental defects (data not shown). In addition to the overall dwarfism, Seckel mice showed a disproportionate decrease in the dimensions of their heads, or microcephaly (**Fig. 2e** and **Supplementary Fig. 1**). Notably, the heads of the mutant mice were not only small but also dysmorphic, showing the micrognathia and receding forehead characteristic of the human disease (**Fig. 2f** and **Supplementary Fig. 1**). While acknowledging the obviously different facial features of mice and humans, we note that the receding forehead phenotype led to the appearance of a protruding nose in $ATR^{S/S}$ mice, which is reminiscent of the "bird-head" phenotype that gave the original name to the disease (**Fig. 2e**).

Consistent with the microcephaly, Seckel mice showed a reduction in the size of their brains (**Supplementary Fig. 2a**). Moreover, magnetic resonance imaging (MRI) analyses revealed profound abnormalities on $ATR^{S/S}$ brains such as the presence of cysts (6/8 mice analyzed) and agenesis of the corpus callosum (AgCC, 8/8 mice) (**Fig. 2g**). These MRI scans are notably similar to those previously obtained from humans with Seckel syndrome[13]. Consistent with the AgCC, histology revealed a severe loss of astrocytes at the corpus callosum of the mutant mice (**Supplementary Fig. 2b**). Together, these findings suggest that the "bird-head" appearance of humans with Seckel syndrome derives from a primary developmental defect in the formation of the brain.

Besides the brain, several organs were noticeably smaller in the mutant mice (**Supplementary Fig. 3a**). Whereas at birth ATR abundance was reduced in all organs, this difference became postnatally attenuated in some of them such as the testes or lungs (**Supplementary Fig. 3b**). This might represent a selection for cells in which the percentage of productive splicing is highest, which will particularly occur in tissues with high replicative indexes. Regardless of its origin, the recovery in ATR abundance suggests an essential role for even minimal amounts of the protein in these organs, as recently described for spermatogenesis in studies performed with a conditional *Atr* allele[14].

The recovery of ATR abundance suggests that the organs in which this was seen could gain a proficient ATR response by adulthood. Accordingly, *in vitro* fertilization could be successfully completed with $ATR^{S/S}$ sperm (data not shown). In contrast, given that all proliferation linked to oogenesis takes place in the embryo, female gametogenesis would not allow postnatal selection for ATR abundance, and a meiotic defect might persist in the adult. Indeed, we obtained no viable oocytes even after hormone-induced superovulation of the mutant mice, and $ATR^{S/S}$ ovaries showed a near-complete absence of maturing oocytes (**Supplementary Fig. 4a**). Although newborn $ATR^{S/S}$ ovaries carried abundant primordial follicles, a high proportion of them were degenerating, which likely indicates a meiotic recombination defect and would explain the later absence of oocytes in the adult (**Supplementary Fig. 4b,c**). None of the phenotypes found in $ATR^{S/S}$ mice were observed in a control strain that carried the same humanized allele without the Seckel mutation (**Fig. 2h,i** and **Supplementary Fig. 5**). And although some of the phenotypic manifestations we observed in $ATR^{S/S}$ mice were in addition to those known in humans, these mice recapitulated all the criteria that are used in the clinic for the diagnosis of Seckel syndrome, including the "bird-headed dwarfism" that originally named the disease.

Development of a progeroid phenotype in Seckel mice

Seckel mice died in less than half a year, showing cachexia and several phenotypes associated with aging, including hair graying, kyphosis, osteoporosis, accumulation of fat in the bone marrow, decreased density of hair follicles and thinner epidermis (**Fig. 3a–d** and data not shown). Analysis of peripheral blood revealed pancytopenia, with decreased numbers of red, white and platelet cells, as it has been reported in humans with Seckel syndrome (**Fig. 3e**)[15]. Altogether, these phenotypes indicate the development of a progeroid syndrome in Seckel mice.

To evaluate whether the aging phenotype was linked to stem cell dysfunction, and due to the presence of pancytopenia, we focused on the hematopoietic stem cell (HSC) compartment—one that is well understood and whose dynamics have been analyzed in relationship to aging[16]. A first indication of a dysfunctional HSC compartment was a general decrease in cellularity and accumulation of fat on $ATR^{S/S}$ bone marrow, which is also observed during normal aging[17]. The analysis of the HSC compartment of the Seckel mice showed similar features to those previously observed in aged mice or humans (**Supplementary Fig. 6a–c**). First, the frequency of LSK ($Lin^-Sca1^+Kit^+$) cells was low in the bone marrow of Seckel mice. Second, within the mutant LSK population, the fraction of long-term HSCs was high and that of multipotent progenitors low[18,19]. In summary, the HSC compartment of young $ATR^{S/S}$ mice resembled that of aged animals.

To determine whether the altered frequencies of $ATR^{S/S}$ HSCs were due to cell-autonomous effects, we performed mixed bone-marrow reconstitution experiments into irradiated wild-type (WT) hosts. In contrast to other mouse models deficient in DNA repair[3], we found

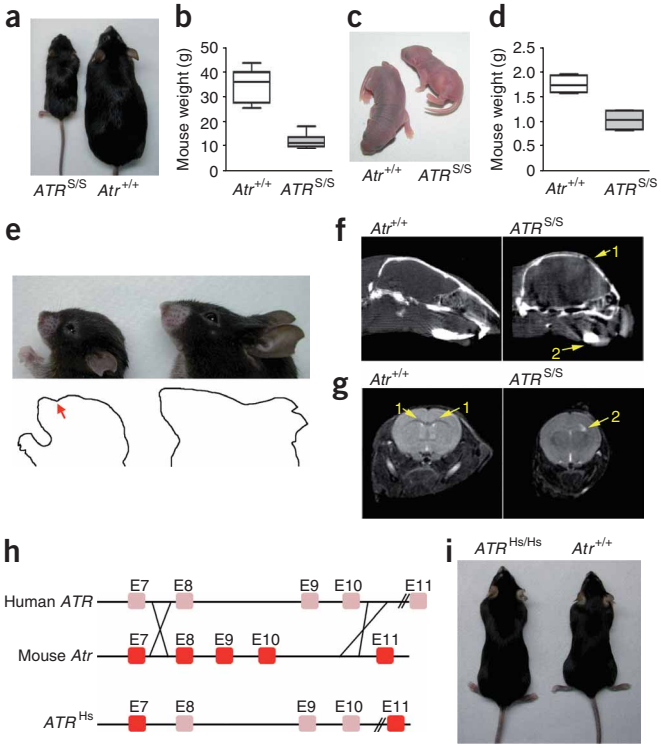

Figure 2 $ATR^{S/S}$ mice recapitulate human Seckel syndrome. (**a**–**d**) Representative pictures and weights of $Atr^{+/+}$ and $ATR^{S/S}$ mice at 3 months of age (**a**,**b**) or at birth (**c**,**d**). $n = 10$ animals per genotype and age, $P < 0.0001$ in both cases. Error bars, s.d.; center lines, medians. (**e**) Picture of the heads of $Atr^{+/+}$ and $ATR^{S/S}$ littermates. An outline is drawn to illustrate the protruding nose (red arrow) due to the receding forehead. (**f**) Computerized tomography of the heads of $Atr^{+/+}$ and $ATR^{S/S}$ littermates illustrating the receding forehead (1) and micrognathia (2). (**g**) MRI scans illustrating the AgCC (corpus callosum, 1) and the presence of cysts (2) in Seckel brains. (**h**) Generation of the control allele (ATR^{Hs}), which is identical to ATR^{S} but lacks the Seckel syndrome mutation. (**i**) Representative picture of 3-month-old $Atr^{+/+}$ and $ATR^{Hs/Hs}$ littermates.

Seckel bone marrow to be equivalent to WT bone marrow in its capacity to reconstitute the granulocyte compartment, and it was also able to substantially reconstitute the lymphocyte compartment (**Supplementary Fig. 6d**,**e**). As $ATR^{S/S}$ HSCs showed repopulating potential when injected into a WT host, but $ATR^{S/S}$ mice developed pancytopenia, non-cell-autonomous factors, such as the deterioration of stem cell niches, must account for the altered function of the HSCs within the mutant mice. The degeneration of the bone marrow in $ATR^{S/S}$ mice also supports this notion that stem cell niches are compromised. Accordingly, reconstitution of Seckel mice with WT bone marrow did not restore normal thymus size (data not shown). In summary, the presence of pancytopenia in $ATR^{S/S}$ mice derives from altered HSC frequencies that resemble those found in aging, which likely result from the degeneration of the niche that supports their function.

Recent studies have shown that human aging triggers a molecular signature characterized by a dampening of the insulin-like growth factor-1–growth hormone (IGF-1/GH) somatotroph axis[20,21], and which is also found in mouse models of progeria[22,23]. Transcriptional profiling of livers and brains of 3-month-old mice revealed such a hallmark in $ATR^{S/S}$ tissues (**Supplementary Fig. 7**). But although the dampening of the IGF-1/GH pathway can also be induced in mice by genotoxic agents[22,23], we did not find a significant increase in the amount of endogenous DNA damage in these organs in postnatal life. This is particularly telling in the case of the brain because, given its nonreplicative nature, ATR should have a limited role in this organ in protecting against postnatal replicative stress. Altogether, our animal, cellular and molecular data demonstrate that the introduction of the Seckel mutation in the mouse led to the development of a progeroid syndrome that limited the lifespan of the animals.

Embryonic ATM/DNAPK-dependent DDR

One possible way to reconcile the dampening of IGF-1/GH in the absence of contemporaneous DNA damage is that this transcriptional program may have been initiated in response to an exposure to DNA damage at a previous stage. To determine the behavior of embryonic cells, we analyzed $Atr^{+/+}$ and $ATR^{S/S}$ MEFs. Like human Seckel cells[11], $ATR^{S/S}$ MEFs were sensitive to ultraviolet or methyl methanesulfonate (**Fig. 4a–c**). Nonetheless, even if they were not exposed to exogenous damage, proliferation of Seckel MEFs decreased sharply and mutant cells rapidly entered senescence (**Fig. 4d**). This occurred regardless of whether the cultures were maintained under normoxic (3% O_2) conditions (data not shown). The growth arrest was concomitant with an accumulation

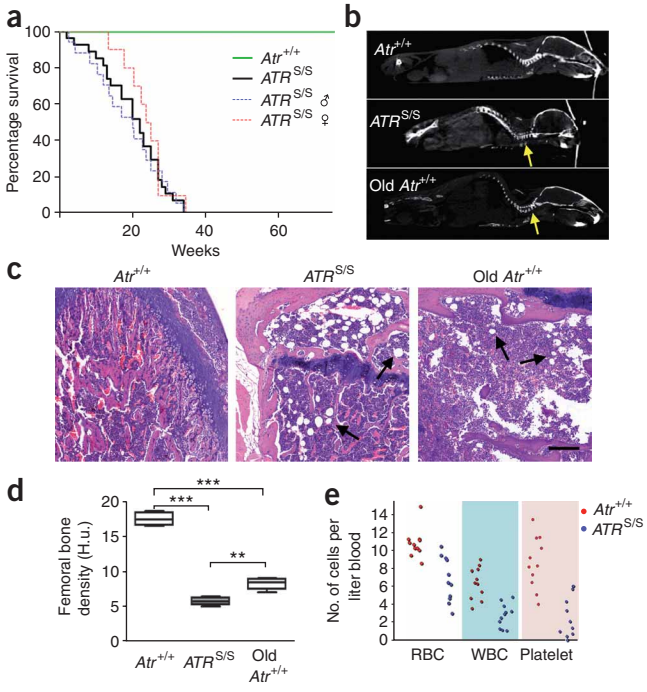

Figure 3 Premature aging of $ATR^{S/S}$ mice. (**a**) Kaplan-Meyer representation of the lifespan of $Atr^{+/+}$ ($n = 20$) and $ATR^{S/S}$ ($n = 27$) mice. (**b**) Computerized tomography of a pair of 2-month-old Seckel and control littermates, as well as an old (25 months) $Atr^{+/+}$ mouse. Yellow arrow, kyphosis. (**c**) Hematoxylin and eosin staining from the femoral head of a pair of 2-month-old Seckel and control male littermates, as well as an old (25 months) $Atr^{+/+}$ male mouse to illustrate the accumulation of fat in the bone marrow (black arrows). Scale bar, 200 μm. (**d**) Distribution of the femoral bone density in $Atr^{+/+}$, $ATR^{S/S}$ and old (25–26 months) $Atr^{+/+}$ mice as a measure of osteoporosis ($n = 7$) per condition; $^{**}P < 0.01$, $^{***}P < 0.001$. Error bars, s.d.; center lines, medians. H.u., Hounsfield unit. We observed no significant differences between the sexes. (**e**) Counts of platelets ($\times 10^{11}$), red blood cells (RBC; $\times 10^{12}$) and white blood cells (WBC; $\times 10^{9}$) obtained from 3-month-old $Atr^{+/+}$ and $ATR^{S/S}$ mice.

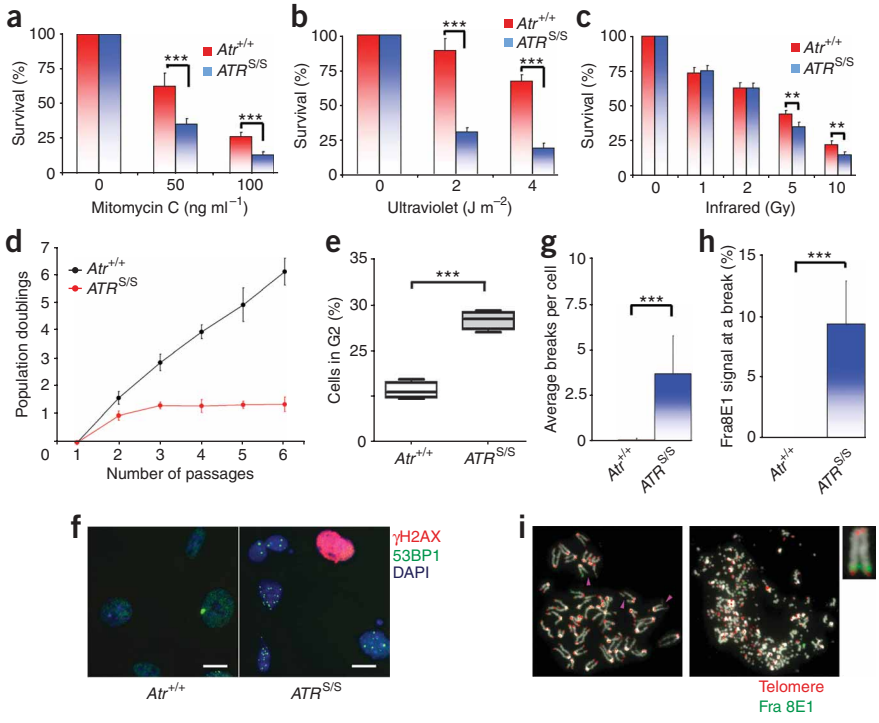

Figure 4 Accumulation of replicative stress in $ATR^{S/S}$ MEFs. (**a**–**c**) Survival of $Atr^{+/+}$ and $ATR^{S/S}$ MEFs in response to mitomycin C (**a**), ultraviolet (**b**) and infrared (**c**). (**d**) Growth curves of $Atr^{+/+}$ and $ATR^{S/S}$ MEFs. (**e**) Percentages of cells at the G2 stage of the cell cycle, derived from the analysis of DNA content by flow cytometry. (**f**) Distribution of γH2AX and 53BP1 on $Atr^{+/+}$ and $ATR^{S/S}$ MEFs. Scale bar, 5 μm. (**g**) Average number of chromosome breaks per cell on control and Seckel metaphases. (**h**) Percentage of the Fra8E1 alleles that were found to be at a break by FISH analyses. (**i**) Representative images of the type of genomic aberrations found on $ATR^{S/S}$ MEFs. Metaphases were stained with probes recognizing the telomeres and the Fra8E1 fragile site. We analyzed 50 metaphases per condition in three replicates. In **a**–**e**,**g**,**h**, error bars, s.d.; center lines, medians; three independent experiments with two independent MEF lines; $^{**}P < 0.01$, $^{***}P < 0.001$.

of cells in G2, suggesting an activation of the DDR due to replicative damage (**Fig. 4e**). Accordingly, a high percentage of $ATR^{S/S}$ MEFs showed pan-nuclear staining for the phosphorylated form of histone H2AX (γH2AX) ($Atr^{+/+}$, 0%; $ATR^{S/S}$, 7.6 ± 2.3%) (**Fig. 4f**). In contrast to γH2AX foci, the pan-nuclear staining of γH2AX was equivalent to that caused by inducers of replicative stress, such as hydroxyurea, and occurred only in cyclin A–expressing cells (data not shown). Many of the mutant cells also showed p53-binding protein-1 (53BP1) foci, indicative of DSBs. Moreover, $ATR^{S/S}$ metaphases had a high frequency of chromosomal breakage which, consistent with the known role of ATR in maintaining the stability of stalled replication forks[24–26] and suppressing fragile site expression[27,28], frequently occurred at fragile sites (**Fig. 4g–i**). Thus, the Seckel MEFs were unable to sustain proliferation *ex vivo* because of the activation of a replicative stress–initiated DDR.

We then investigated which kinase was responsible for activating the DDR in $ATR^{S/S}$ MEFs. A combined treatment with inhibitors of ATM and of the DNA-dependent protein kinase catalytic subunit (DNAPKcs) virtually eliminated the γH2AX signal—and 53BP1 foci—in Seckel cells (**Fig. 5a**,**b**). We thus tested whether the use of the inhibitors could alleviate the growth arrest. However, whereas treatment with the inhibitors abrogated the G2 arrest (**Fig. 5c**), this did not restore growth. On the contrary, ATM and DNAPKcs inhibitors were particularly toxic for Seckel MEFs (**Fig. 5d**). Consistent with the synthetic lethal effects observed *in vitro*, ATM deficiency led to embryonic lethality when combined with the $ATR^{S/S}$ genotype (data not shown). In summary, the severe downregulation of ATR in MEFs leads to the activation of

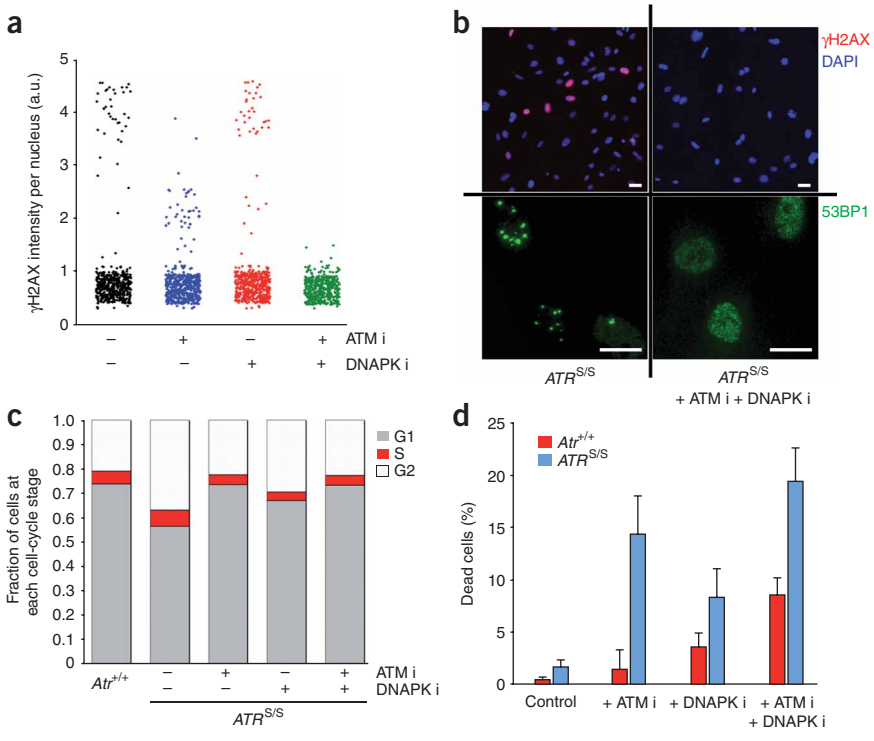

Figure 5 Response of $ATR^{S/S}$ MEFs to PIKK inhibitors. (**a**) High-throughput microscopy data illustrating the distribution of γH2AX signal in $ATR^{S/S}$ MEFs treated with ATM and DNAPK inhibitors (i). A.u., arbitrary units. (**b**) Representative images from the analysis shown in **a** in the absence (left) or presence (right) of both drugs (top), along with the distribution of 53BP1 (bottom). Scale bars, 5 μm. (**c**) Effect of the inhibitors on the G2 arrest observed in WT and $ATR^{S/S}$ MEFs. Experiments performed three times with two independent MEF lines; graph shows population distribution in one representative experiment. (**d**) Percentages of dead cells found in WT and $ATR^{S/S}$ MEF cultures after 24 h of treatment with the inhibitors. Error bars, s.d. from three independent experiments with two independent MEF lines; $P < 0.001$ in all $Atr^{+/+}$ versus $ATR^{S/S}$ conditions.

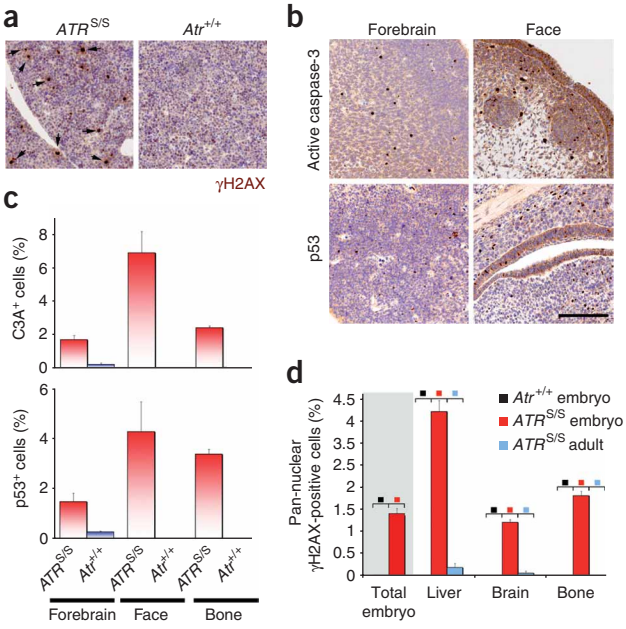

Figure 6 Accumulation of replicative stress on $ATR^{S/S}$ embryos. (**a**) Immunohistochemistry for γH2AX in the liver of 13.5 d.p.c. WT and Seckel littermate embryos. (**b**) Examples of two representative areas of $ATR^{S/S}$ embryos, chosen from organs that appear compromised on adult mice, such as the forebrain or the face, that illustrate the generalized accumulation of p53 or apoptotic cells (as measured with activated caspase-3) in the mutant embryos. Scale bar (applies to **a** and **b**), 150 μm. (**c**) Quantification of the signals from **b**. C3A, activated caspase-3. (**d**) Quantification of the frequency of cells with pan-nuclear γH2AX in different organs of 13.5 d.p.c. embryos and 2-month-old mice. Colored squares indicate the genotype and age for each bar. Error bars, s.d.; $P < 0.001$ in all pairwise comparisons of $Atr^{+/+}$ versus $ATR^{S/S}$ tissues in **c**,**d**, as well as between all embryo and adult $ATR^{S/S}$ tissues compared in **d** ($n = 5$ in all cases).

an ATM- and DNAPKcs-dependent DDR in replicating cells owing to an accumulation of replicative stress.

Accumulation of replicative stress in Seckel embryos

We then evaluated whether evidence of replicative stress could also be detected *in vivo*. To this end, γH2AX distribution was analyzed in 13.5 days post coitum (d.p.c.) embryos (**Supplementary Fig. 8**; **Fig. 6a**). Whereas almost no γH2AX is normally detected in WT embryos, $ATR^{S/S}$ littermates showed an accumulation of cells with pan-nuclear γH2AX throughout the entire embryo. p53 and activated caspase-3 showed a similar distribution, as proof that many cells were being eliminated by apoptosis at this stage (**Fig. 6b**,**c**). A similar analysis only revealed a marginal increase of replicative stress or apoptosis in tissues from adult mutant mice such as the brain, colon, proliferating B cells, stomach, liver, lung, kidneys, skin and heart (**Fig. 6d** and data not shown). This observation could reflect the high replicative activity of embryonic stages in contrast to adult tissues. One exception to this occurred in the brain, which undergoes a rapid proliferative burst in the first days of life. In this case, both embryonic and newborn brains showed apoptosis and replicative stress in the replicating areas (**Fig. 7a–c**). In contrast, we observed no proliferation or differentiation defects (**Fig. 7d**). It is likely that this particular proliferative expansion of the brain will contribute to the microcephaly of the mutant mice through the effects of replicative stress–driven apoptosis. Altogether, our data revealed that Seckel embryos show a generalized activation of an apoptotic DDR that, with the exception of the newborn brain, becomes marginal in postnatal life.

p53 deficiency accelerates aging in Seckel mice

Given the accumulation of p53 in Seckel embryos, we tested whether p53 deficiency could mitigate some of the aging phenotypes of $ATR^{S/S}$ mice. Unexpectedly, $ATR^{S/S}$; $Trp53^{-/-}$ double-mutant mice were rarely born (1.02% from $ATR^{S/+} \times Trp53^{+/-}$ crosses, $n = 294$), and the few mice that were born showed a more severe progeroid syndrome than their $ATR^{S/S}$; $Trp53^{+/+}$ littermates (**Supplementary Fig. 9**). As a consequence, no $ATR^{S/S}$; $Trp53^{-/-}$ mice survived for more than 2 months.

To determine the molecular mechanism by which p53 deficiency exacerbated the Seckel phenotype, we infected MEFs with control and *Trp53* short hairpin RNA (shRNA)-expressing retroviruses. Whereas p53 downregulation in WT MEFs slightly increased their growth, it led to a loss of viability of the mutant cultures accompanied by massive nuclear abnormalities (**Fig. 8a**,**b**). One possibility was that p53 loss could be driving G2-arrested cells to mitotic catastrophe. But to the contrary, p53 depletion in $ATR^{S/S}$ MEFs led to a further accumulation of cells in G2 as well as a fourfold increase in the number of cells showing pan-nuclear γH2AX staining, indicating that the increased growth rates associated with p53 loss had led to an increase of replicative stress on Seckel cells (**Fig. 8c**,**d**). If p53 loss occurs in ATR-proficient cells, these cells should still be able to deal with the higher replication rates and to avoid the development of replicative stress. Accordingly, whereas $Trp53^{-/-}$ embryos did not show evidences of replicative stress (**Supplementary Fig. 10**), $ATR^{S/S}$; $Trp53^{-/-}$ embryos showed a marked increase of cells with pan-nuclear γH2AX compared with their $ATR^{S/S}$; $Trp53^{+/+}$ littermates (**Fig. 8e**,**f**). Moreover, p53 deficiency further increased the number of cells that were eliminated by apoptosis in Seckel embryos, which explains the

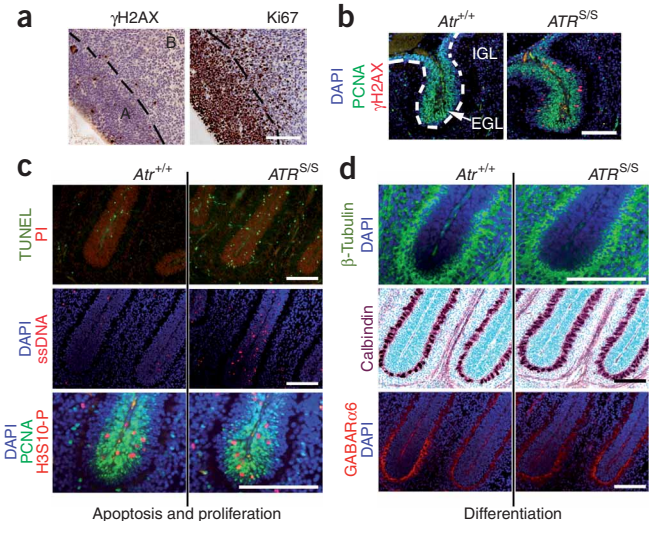

Figure 7 Replicative stress–driven apoptosis in proliferating areas of the developing brain. (**a**) γH2AX and KI67 immunohistochemistry on sections of the developing brain of 13.5 d.p.c. $ATR^{S/S}$ embryos. The presence of γH2AX was restricted to areas of active neurogenesis in the ventricular zone (A), little signal being detected in the nonproliferating subventricular areas (B). (**b**) Presence of replicative stress in the actively replicating external germinal layer (EGL) of p6 Seckel cerebellum. IGL, internal germinal layer. (**c**) Proliferation (as measured by PCNA or H3-S10P) and apoptosis (as measured by TUNEL or ssDNA) on $Atr^{+/+}$ or $ATR^{S/S}$ cerebella. (**d**) Cerebellar differentiation was not substantially affected in Seckel mice (as measured with β-tubulin, calbindin and GABARα6).

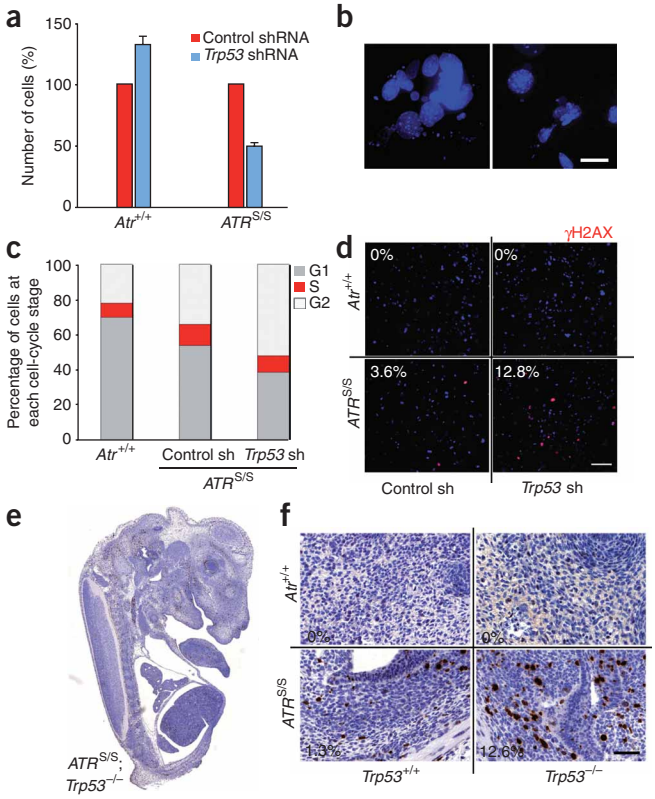

Figure 8 Effect of p53 depletion on $ATR^{S/S}$ cells and mice. (**a**) Relative number of cells alive in $Atr^{+/+}$ and $ATR^{S/S}$ cultures after p53 depletion (see Online Methods). The number was normalized to cells infected with a control shRNA–expressing (sh) lentivirus. Error bars, s.d.; three independent experiments with two independent MEF lines. $P < 0.001$ in the pairwise comparisons of control and p53-targeting shRNAs. (**b**) Representative images of the type of abnormal nuclei found on p53-depleted Seckel MEFs. Scale bar, 5 μm. (**c**,**d**) Effect of p53 depletion on the G2 arrest (**c**) and γH2AX accumulation (**d**) observed on $ATR^{S/S}$ MEFs. Experiments performed three times with two independent MEF lines; graph shows population distribution in one representative experiment. Scale bar, 100 μm. (**e**) γH2AX immunohistochemistry on a sagittal section of a 13.5 d.p.c. $ATR^{S/S}$; $Trp53^{-/-}$embryo. (**f**) Magnification of a region close to the jaw on embryos from the various genotypes, processed as in **e**. Scale bar, 50 μm.

increased dwarfism of the double-mutant mice (data not shown). In summary, the loss of p53 led to an increase in the amount of replicative stress suffered by Seckel embryos, which led to an aggravation of the Seckel phenotypes and further accelerated the onset of aging in $ATR^{S/S}$ mice.

DISCUSSION

The Seckel strain developed in this study recapitulates the human disease to a remarkable extent. In addition to the overall appearance, the previously reported observations of chromosomal instability[15,28–30], progeria or senile appearance[15,31–33] and pancytopenia[15] were all present in Seckel mice. Characterization of this mouse model also suggests possible mechanisms for some of the Seckel syndrome phenotypes. These included a specific depletion of astrocytes at the corpus callosum as an explanation for the AgCC, the degeneration of the bone marrow and associated HSC dysfunction as the cause of pancytopenia, and the generalized activation of an apoptotic DDR in the embryo as an explanation for the dwarfism. Of particular relevance is the finding that microcephaly could be, at least in part, explained by the exponential replicative expansion that the brain undergoes in the first days of life, which makes it more susceptible to mutations that promote replicative stress.

Seckel syndrome is a variegated disease that has been mapped to four different loci, from which only two genes—*ATR* and *PCNT*, encoding pericentrin—have been identified[11,34]. The severity of the phenotypes might therefore differ from case to case. In addition to the phenotypes described above, individuals with *ATR*-Seckel syndrome have shown microcrania with fused sutures, dental malocclusion and deficient closure of the fontalelles[35], all of which were frequent in $ATR^{S/S}$ mice (see **Supplementary Fig. 2**). Although no pancytopenia was reported, the subjects were infants at the time of analysis and such a symptom might develop later. Altogether, we believe the mouse mutant generated in this study constitutes a valid model for the investigation of Seckel syndrome in the laboratory.

In previously published progeroid models, DNA damage accumulates after birth[1,3]. However, whereas we found a generalized activation of the DDR in $ATR^{S/S}$ embryos, we did not detect a similar increase of endogenous damage on adult tissues. On the basis of this observation, we propose that the accumulation of replicative stress in the embryo affects the future onset of aging and overall well being of the adult mice. This is supported by several arguments. First, organs that are highly proliferative in postnatal mice undergo a selection process so that ATR abundance in Seckel mice becomes close to that in WT. Thus, even if adult $ATR^{S/S}$ mice are ATR proficient in many of their regenerating organs, this does not prevent the onset of progeria. This is in agreement with the normal functioning of $ATR^{S/S}$ sperm or HSCs when transplanted into a WT host. Second, adult organs with embryonic replicative stress but no evidence of DNA damage in postnatal life show a transcriptional signature characteristic of 'aged' organs. Of note, this transcriptional response is activated by the exposure to DNA damage[22,23]. Finally, even though the elimination of ATR in 1-month-old mice leads to the development of several progeroid symptoms[14], some of these mice can survive for up to 19 months (E. Brown, personal communication). This comparison by itself strongly suggests that embryonic ATR deficiency substantially affects future lifespan. One possible way to explain this phenomenon is that the generalized loss of cells by apoptosis during embryogenesis can compromise future stem cell functioning, not only by limiting stem cell pools but particularly by an alteration of stem cell niches, as we have seen in the case of HSCs. Altogether, we propose that the generalized exposure to DNA damage in $ATR^{S/S}$ embryos is responsible for the initiation of a progeroid program that drives young animals into senescence.

The concept of embryonic dysfunction leading to problems in adulthood has previously been described as 'intrauterine programming'[36–38]. Among other things, intrauterine programming has been associated to the onset of type-2 diabetes, obesity, hypertension, cardiac dysfunction, kidney disorders, autoimmunity and osteoporosis. Since the 1920s, a decreased size of the head and brain accompanied by mental retardation has been known to be the main effect of fetal exposure to DNA damage[39]. Furthermore, intrauterine radiation leads to AgCC in Swiss mice[40]. Notably, the main consequence of prenatal exposure of rats to replicative stress–inducing agents such as hydroxyurea is the presence of several craniofacial malformations, including micrognathia, which is a hallmark of Seckel syndrome[40]. Nevertheless, these works evaluated the effects of acute intrauterine exposure to genotoxic agents, so it is likely that a prolonged exposure, as in the case of $ATR^{S/S}$ embryos, could lead to more prominent and lasting effects. We therefore suggest adding aging to the list of adult phenotypic manifestations that can arise as a consequence of intrauterine distress.

Previous mouse models of progeria have shown that the absence of p53 relieves some of the growth disadvantages and, if no cancer arises,

enhances the lifespan of these animals[41]. Unexpectedly, we found here that p53 loss accelerates the aging of Seckel mice. The explanation for this phenomenon seems to lie in the effects of p53 on cell cycle progression. As some of the p53 targets, such as p21, are well known inhibitors of cyclin-dependent kinase activity[42], it is reasonable to think that p53 loss might enable slightly faster replication. Whereas ATR-proficient cells might be able to cope with this, it would exacerbate the accumulation of replicative stress when ATR signaling is compromised. Notably, p53 loss further increased the amount of apoptosis of Seckel embryos, suggesting that replicative stress might be able to initiate p53-independent apoptotic pathways. Along these lines, a recent work revealed that loss of the checkpoint kinase Chk1 leads to p53-independent apoptosis in zebrafish[43].

Besides its implications for aging, the synthetic lethal effects of ATR and p53 suggest that ATR inhibitors could be explored for the selective elimination of p53-deficient tumors. Similarly, our results can also help to explain the increased sensitivity of p53-deficient tumors to UCN-01, a chemical inhibitor of the ATR target Chk1 (ref. 44). It is reasonable to think that the synthetic lethal effects of ATR or Chk1 with p53 loss will also apply to other genetic changes that promote faster replication rates, as is the case in many cancer-associated mutations. In this regard, a recent report has shown that p21 loss in the context of an oncogene that generates replication-linked DNA damage is tumor suppressive[45]. Thus, in the context of replicative stress, mutations that promote proliferation will boost replicative stress even further, which, if too high, can limit the viability of the cells. Of note, this is not the first evidence of an aging-suppressive function of the p53 response: transgenic mice carrying extra alleles encoding p53 and $p19^{ARF}$ have been shown to have an increase in the median lifespan[46]. However, our data provide the first genetic evidence showing that p53 loss might promote aging *in vivo*.

Death of Seckel mice was associated with a generalized organ failure, with several organs showing phenotypes that are reminiscent of age-related dysfunction. Nevertheless, even though ATR has been shown to be a haploinsufficient tumor suppressor[47], we detected no tumors in $ATR^{S/S}$ mice, even in the absence of p53. One potential explanation is that the toxic effects of high levels of replicative stress may counterbalance the mutagenicity of DNA breaks. In this manner, whereas a small reduction in ATR might promote cancer, a severe dampening of the ATR response might become tumor suppressive. Similarly, although Chk1 is a haploinsufficient tumor suppressor[48], Chk1 inhibitors are now being used to kill cancer cells. One example of such a dichotomy is XPF, mild mutations in which increase cancer susceptibility, whereas mutations that further compromise activity promote progeria[23].

In summary, we here present a mouse model of the ATR-Seckel syndrome that faithfully recapitulates the symptoms of the human disease and provides a viable model for genetic studies of ATR function in a mammal. Our study suggests a mechanism whereby Seckel arises as a consequence of the accumulation of replicative stress during embryonic development, which triggers an ATM-dependent DDR that affects phenotypes in the adult mice. We believe that incorporating aging into the battery of phenotypes that can be influenced by fetal distress might help to understand the variability of the aging process that is observed between individuals.

METHODS

Methods and any associated references are available in the online version of the paper at http://www.nature.com/naturegenetics/.

Note: Supplementary information is available on the Nature Genetics website.

ACKNOWLEDGMENTS

We thank M. Serrano and A. Ramiro for critical comments on the manuscript. We also thank S.P. Jackson for his help with the PIKK inhibitors and A. Garcia for cytometry. M.M. is supported by a Ramón y Cajal contract from the Spanish Ministry of Science (RYC-2003-002731) and from a grant from Fondo de Investigaciones Sanitarias (PI080220). Work in O.F.-C.'s laboratory is supported by grants from the Spanish Ministry of Science (RYC-2003-002731, CSD2007-00017 and SAF2008-01596), European Molecular Biology Organization Young Investigator Programme, European Research Council (ERC-210520) and Epigenome Network of Excellence.

AUTHOR CONTRIBUTIONS

O.F.-C. designed the study and experiments and wrote the paper. M.M. performed most of the experiments presented. M.F.M. and R.S. helped in the analysis of Seckel MEFs and embryos. S.B. and A.N. performed HSC and chromosomal breakage analyses. F.M. helped with the whole body Imaging. M.C. helped with the pathology. Y.L. and P.J.M. performed the analyses of the brains.

Published online at http://www.nature.com/naturegenetics/.
Reprints and permissions information is available online at http://npg.nature.com/reprintsandpermissions/.

1. Lombard, D.B. *et al.* DNA repair, genome stability, and aging. *Cell* **120**, 497–512 (2005).
2. Sedelnikova, O.A. *et al.* Senescing human cells and ageing mice accumulate DNA lesions with unrepairable double-strand breaks. *Nat. Cell Biol.* **6**, 168–170 (2004).
3. Rossi, D.J. *et al.* Deficiencies in DNA damage repair limit the function of haematopoietic stem cells with age. *Nature* **447**, 725–729 (2007).
4. Schumacher, B., Garinis, G.A. & Hoeijmakers, J.H. Age to survive: DNA damage and aging. *Trends Genet.* **24**, 77–85 (2008).
5. Harper, J.W. & Elledge, S.J. The DNA damage response: ten years after. *Mol. Cell* **28**, 739–745 (2007).
6. Xu, Y. & Baltimore, D. Dual roles of ATM in the cellular response to radiation and in cell growth control. *Genes Dev.* **10**, 2401–2410 (1996).
7. Elson, A. *et al.* Pleiotropic defects in ataxia-telangiectasia protein-deficient mice. *Proc. Natl. Acad. Sci. USA* **93**, 13084–13089 (1996).
8. Barlow, C. *et al.* Atm-deficient mice: a paradigm of ataxia telangiectasia. *Cell* **86**, 159–171 (1996).
9. Brown, E.J. & Baltimore, D. Essential and dispensable roles of ATR in cell cycle arrest and genome maintenance. *Genes Dev.* **17**, 615–628 (2003).
10. de Klein, A. *et al.* Targeted disruption of the cell-cycle checkpoint gene ATR leads to early embryonic lethality in mice. *Curr. Biol.* **10**, 479–482 (2000).
11. O'Driscoll, M., Ruiz-Perez, V.L., Woods, C.G., Jeggo, P.A. & Goodship, J.A. A splicing mutation affecting expression of ataxia-telangiectasia and Rad3-related protein (ATR) results in Seckel syndrome. *Nat. Genet.* **33**, 497–501 (2003).
12. Seckel, H. *Bird-Headed Dwarfs: Studies in Developmental Anthropology Including Human Proportions* (Karger, Basel, Switzerland, 1960).
13. Shanske, A., Caride, D.G., Menasse-Palmer, L., Bogdanow, A. & Marion, R.W. Central nervous system anomalies in Seckel syndrome: report of a new family and review of the literature. *Am. J. Med. Genet.* **70**, 155–158 (1997).
14. Ruzankina, Y. *et al.* Deletion of the developmentally essential gene ATR in adult mice leads to age-related phenotypes and stem cell loss. *Cell Stem Cell* **1**, 113–126 (2007).
15. Butler, M.G., Hall, B.D., Maclean, R.N. & Lozzio, C.B. Do some patients with Seckel syndrome have hematological problems and/or chromosome breakage? *Am. J. Med. Genet.* **27**, 645–649 (1987).
16. Rossi, D.J., Jamieson, C.H. & Weissman, I.L. Stems cells and the pathways to aging and cancer. *Cell* **132**, 681–696 (2008).
17. Rosen, C.J. & Bouxsein, M.L. Mechanisms of disease: is osteoporosis the obesity of bone? *Nat. Clin. Pract. Rheumatol.* **2**, 35–43 (2006).
18. Morrison, S.J., Wandycz, A.M., Akashi, K., Globerson, A. & Weissman, I.L. The aging of hematopoietic stem cells. *Nat. Med.* **2**, 1011–1016 (1996).
19. Sudo, K., Ema, H., Morita, Y. & Nakauchi, H. Age-associated characteristics of murine hematopoietic stem cells. *J. Exp. Med.* **192**, 1273–1280 (2000).
20. Bartke, A. Minireview: role of the growth hormone/insulin-like growth factor system in mammalian aging. *Endocrinology* **146**, 3718–3723 (2005).
21. Lombardi, G., Di Somma, C., Rota, F. & Colao, A. Associated hormonal decline in aging: is there a role for GH therapy in aging men? *J. Endocrinol. Invest.* **28**, 99–108 (2005).
22. van der Pluijm, I. *et al.* Impaired genome maintenance suppresses the growth hormone–insulin-like growth factor 1 axis in mice with Cockayne syndrome. *PLoS Biol.* **5**, e2 (2007).
23. Niedernhofer, L.J. *et al.* A new progeroid syndrome reveals that genotoxic stress suppresses the somatotroph axis. *Nature* **444**, 1038–1043 (2006).
24. Cha, R.S. & Kleckner, N. ATR homolog Mec1 promotes fork progression, thus averting breaks in replication slow zones. *Science* **297**, 602–606 (2002).

25. Sogo, J.M., Lopes, M. & Foiani, M. Fork reversal and ssDNA accumulation at stalled replication forks owing to checkpoint defects. *Science* **297**, 599–602 (2002).
26. Stiff, T. *et al.* Nbs1 is required for ATR-dependent phosphorylation events. *EMBO J.* **24**, 199–208 (2005).
27. Casper, A.M., Nghiem, P., Arlt, M.F. & Glover, T.W. ATR regulates fragile site stability. *Cell* **111**, 779–789 (2002).
28. Casper, A.M., Durkin, S.G., Arlt, M.F. & Glover, T.W. Chromosomal instability at common fragile sites in Seckel syndrome. *Am. J. Hum. Genet.* **75**, 654–660 (2004).
29. Bobabilla-Morales, L. *et al.* Chromosome instability induced in vitro with mitomycin C in five Seckel syndrome patients. *Am. J. Med. Genet. A.* **123A**, 148–152 (2003).
30. Syrrou, M., Georgiou, I., Paschopoulos, M. & Lolis, D. Seckel syndrome in a family with three affected children and hematological manifestations associated with chromosome instability. *Genet. Couns.* **6**, 37–41 (1995).
31. Arnold, S.R., Spicer, D., Kouseff, B., Lacson, A. & Gilbert-Barness, E. Seckel-like syndrome in three siblings. *Pediatr. Dev. Pathol.* **2**, 180–187 (1999).
32. Boscherini, B. *et al.* Intrauterine growth retardation. A report of two cases with bird-headed appearance, skeletal changes and peripheral GH resistance. *Eur. J. Pediatr.* **137**, 237–242 (1981).
33. Fathizadeh, A., Soltani, K., Medenica, M. & Lorincz, A.L. Pigmentary changes in Seckel's syndrome. *J. Am. Acad. Dermatol.* **1**, 52–54 (1979).
34. Griffith, E. *et al.* Mutations in pericentrin cause Seckel syndrome with defective ATR-dependent DNA damage signaling. *Nat. Genet.* **40**, 232–236 (2008).
35. Goodship, J. *et al.* Autozygosity mapping of a Seckel syndrome locus to chromosome 3q22. 1-q24. *Am. J. Hum. Genet.* **67**, 498–503 (2000).
36. Fowden, A.L., Giussani, D.A. & Forhead, A.J. Intrauterine programming of physiological systems: causes and consequences. *Physiology (Bethesda)* **21**, 29–37 (2006).
37. Fowden, A.L., Forhead, A.J., Coan, P.M. & Burton, G.J. The placenta and intrauterine programming. *J. Neuroendocrinol.* **20**, 439–450 (2008).
38. Barker, D. The fetal origins of adult disease. *Proc. R. Soc. Lond. B* **262**, 37–43 (1995).
39. Murphy, D.P. Ovarian radiation—its effect on the health of subsequent children. Review of the literature, experimental and clinical, with a report of 320 human pregnancies. *Surg. Gynecol. Obstet.* **47**, 201–215 (1928).
40. Schmidt, S.L. & Lent, R. Effects of prenatal irradiation on the development of cerebral cortex and corpus callosum of the mouse. *J. Comp. Neurol.* **264**, 193–204 (1987).
41. Rodier, F., Campisi, J. & Bhaumik, D. Two faces of p53: aging and tumor suppression. *Nucleic Acids Res.* **35**, 7475–7484 (2007).
42. el-Deiry, W.S. *et al.* WAF1, a potential mediator of p53 tumor suppression. *Cell* **75**, 817–825 (1993).
43. Sidi, S. *et al.* Chk1 suppresses a caspase-2 apoptotic response to DNA damage that bypasses p53, Bcl-2, and caspase-3. *Cell* **133**, 864–877 (2008).
44. Wang, Q. *et al.* UCN-01: a potent abrogator of G2 checkpoint function in cancer cells with disrupted p53. *J. Natl. Cancer Inst.* **88**, 956–965 (1996).
45. Viale, A. *et al.* Cell-cycle restriction limits DNA damage and maintains self-renewal of leukaemia stem cells. *Nature* **457**, 51–56 (2009).
46. Matheu, A. *et al.* Delayed ageing through damage protection by the Arf/p53 pathway. *Nature* **448**, 375–379 (2007).
47. Brown, E.J. & Baltimore, D. ATR disruption leads to chromosomal fragmentation and early embryonic lethality. *Genes Dev.* **14**, 397–402 (2000).
48. Liu, Q. *et al.* Chk1 is an essential kinase that is regulated by Atr and required for the G_2/M DNA damage checkpoint. *Genes Dev.* **14**, 1448–1459 (2000).

ONLINE METHODS

Mice, MEFs and human cells. All mice were kept in a specific pathogen–free barrier zone. Targeting constructs for the generation of humanized $ATR^{S/S}$ and $ATR^{Hs/Hs}$ alleles were generated by recombineering (Genebridges). p53-deficient mice have been described[49]. MEFs were isolated from 12.5 d.p.c. embryos. Survival was determined by Trypan blue exclusion 5 d after the exposure to infrared or 2 d after exposure to mitomycin C or ultraviolet. RT-PCR at the exon 8–exon 10 boundary was performed with primers described before[11]. ATM and DNAPKcs inhibitors were kindly provided by M. O'Connor (AstraZeneca UK) and used at 50 nM and 5 μM, respectively. Human control and ATR-Seckel fibroblast lines have been described before and were a kind gift from M. O'Driscoll (University of Sussex Centre for Genome Damage and Stability)[11]. Control and p53-targeting shRNAs were a kind gift from J.M. Silva (Columbia University).

Metaphase analysis. Telomere repeats were detected by hybridization of a Cy3-conjugated PNA probe. Biotinylated probe for Fra8E1 was prepared by nick translation of a BAC (gift of T. Glover, University of Michigan).

Immunofluorescence and immunoblotting. We used antibodies to γH2AX (Upstate Biotechnology), ATR (Serotec), 53BP1 (Novus Biologicals), p53 (Novocastra), as well as secondary antibodies conjugated with Alexa 488 or Alexa 594 (Molecular Probes). High-throughput microscopy–mediated analysis of the DDR has been described before[50]. Protein blot analyses were performed on the LICOR platform (Biosciences).

Immunohistochemistry. 13.5 d.p.c. embryos were fixed in formalin and embedded in paraffin for subsequent processing. Consecutive 2.5-μm sections were treated with citrate for antigen recovery and processed for immunohistochemistry with antibodies to γH2AX (Upstate), p53 (Novocastra) and activated caspase-3 (R&D Systems). Hematoxylin was used to counterstain. Whole-embryo immunohistochemistry samples were scanned with a MIRAX digitalized system (Zeiss), and the digitized images are available upon request.

Whole-body imaging. Whole-body imaging was performed on anesthetized mice using the eXplore Vista PET-CT (GE Healthcare) and a 7-tesla Pharmascan (Bruker). MMWKS software (GE Healthcare) was used to quantify the mineral density in the femur.

Gene expression of the IGF-1/GH factors. Total RNA was hybridized with Agilent 4x44K mouse microarray slides (Agilent Technologies) according to the manufacturer's instructions. The assay was performed in duplicate, with dye swapping to compensate for labeling biases. The data for the genes of the IGF-1/GH previously associated to progeria[22,23] are presented in **Supplementary Figure 7**.

Brain histology and immunohistochemistry. Brain tissues were drop-fixed in 4% PBS-buffered paraformaldehyde at postnatal day 6. Fixed brains were then treated with PBS-buffered 25% (wt/vol) sucrose solution and cryosectioned at 10 μm using an HM500M cryostat (Microm). Nissl staining was done using 1% thionin (Sigma) in 0.1% acetic acid. Primary antibodies used for this study were those to calbindin-D28K (1:2,000, Sigma), GABARa6 (1:500, Chemicon), β-tubulin III (clone Tuj1, 1:1,000, BabCo), PCNA (1:500, Santa Cruz Biotechnology), γH2AX (1:500, Cell Signaling Technology), H3-pSer10 (1:2,000, Cell Signaling) and GFAP (1:500, Sigma). Citrate based antigen retrieval method was applied to all primary antibodies. Apoptosis was measured using ssDNA antibodies (1:300, IBL) or TUNEL using Apoptag (Chemicon International) according to the manufacturer's instructions.

49. Jacks, T. *et al.* Tumor spectrum analysis in p53-mutant mice. *Curr. Biol.* **4**, 1–7 (1994).
50. Murga, M. *et al.* Global chromatin compaction limits the strength of the DNA damage response. *J. Cell Biol.* **178**, 1101–1108 (2007).